RSC Advances

PAPER

View Article Online
View Journal | View Issue

Cite this: *RSC Adv.*, 2021, **11**, 9542

Investigation of the solid–liquid ternary phase diagrams of 2HNIW·HMX cocrystal†

Qian Jia,‡[a] Jia Wang,‡[a] Shijie Zhang,[a] Jiaoqiang Zhang,*[a] Ning Liu*[b] and Kaichang Kou*[a]

The influence of temperature and solvent on the solid–liquid ternary phase diagrams of the 2HNIW·HMX cocrystal has been investigated. Ternary phase diagrams were constructed for the 2HNIW·HMX cocrystal in acetonitrile and ethyl acetate at 15 °C and 25 °C. HMX and HNIW showed inconsistent dissolution behavior and congruent dissolution behavior in acetonitrile and ethyl acetate, respectively. In the HMX–HNIW–acetonitrile system, the 2HNIW·HMX cocrystal has a narrow thermodynamically stable region at both temperatures. The cocrystal exhibits a wider thermodynamically stable region in the HMX–HNIW–ethyl acetate system. The results show that the choice of solvent has a crucial influence on the dissolution behavior of the cocrystal and the size and position of each region in the phase diagram, while the temperature has no apparent effect on the overall appearance of the phase diagram. By properly selecting the ratios, the 2HNIW·HMX cocrystal could be prepared by the isothermal slurry conversion crystallization method.

Received 4th January 2021
Accepted 20th February 2021

DOI: 10.1039/d1ra00057h

rsc.li/rsc-advances

Introduction

A cocrystal is a combination of two or more compounds, which are combined in the same crystal lattice with a defined stoichiometric ratio relying on non-covalent interactions (hydrogen bonds, π–π stacking and van der Waals forces), and has solid-state properties different from those of the pure component materials or simple physical mixtures.[1–3] Recently, co-crystallization, the method of mixing different single compounds into cocrystals at the molecular level, has attracted more and more attention in the field of energetic materials.[4–7] For energetic materials, high energy is always accompanied by poor sensitivity.[8–11] Cocrystallization has become one of the effective methods to develop energetic materials with high energy and insensitivity.[12] Compared with single compounds, cocrystal materials can effectively change the physicochemical properties such as density, solubility, and stability through co-crystallization.[13–15] In addition, cocrystal explosives can effectively improve the safety of energetic materials and reduce the sensitivity of explosives, thereby solving the contradiction between the energy and sensitivity of explosives.[16–19]

2,4,6,8,10,12-Hexanitro-2,4,6,8,10,12-hexazisowurtzitane (HNIW), also known as CL-20, is a comparatively new energetic compound with high density, large enthalpy of formation, excellent oxygen balance, and high detonation velocity.[20–22] It is regarded as one of the most potent explosives nowadays, while the application of HNIW is currently restricted due to its high sensitivity towards friction, impact, and electric spark.[23,24] 1,3,5,7-Tetranitro-1,3,5,7-tetrazocane (HMX) is an explosive compound with good thermal stability, and it possesses greater explosive power than most energetic materials.[25] 2HNIW·HMX (in a 2 : 1 molar ratio) cocrystal was first synthesized by Dr Bolton, which exhibited high explosive power and owned a higher oxygen balance.[26]

Currently, solvent crystallization, spray drying, and grinding are the commonly used techniques to obtain explosive cocrystals.[27–30] However, it is difficult to apply the spray drying method and the grinding method to the development of industrial-scale manufacturing of cocrystal. Therefore, the solvent crystallization method has become the preferred method for industrial cocrystal preparation. The ternary phase diagram can be used as a guide for choosing a suitable solvent or a synthetic method for cocrystal formation and provides a basis for the development of industrial-scale preparation procedures using solution crystallization.[31,32]

Ternary phase diagrams can easily show any point represents a fixed composition of the three substances. The phase behavior of the two pure components in the solvent can provide insights into the thermodynamically stable region of each phase and the co-crystallization process.[33–35] From our previous work experience, the size and position of the thermodynamically stable region of the cocrystal phase depend on the choice of solvent.[36] Whether it is a pure solvent or a mixture solvent system, the symmetry of the phase diagram depends on the solubility of two pure components in the selected solvent system. If the two pure components have a large solubility difference in the selected

[a]*Shaanxi Key Laboratory of Macromolecular Science and Technology, School of Chemistry and Chemical Engineering, Northwestern Polytechnical University, Xi'an, Shaanxi, 710072, China. E-mail: zhangjq@nwpu.edu.cn; koukc@nwpu.edu.cn*

[b]*Xi'an Modern Chemistry Institute, Xi'an, Shaanxi, 710065, China*

† Electronic supplementary information (ESI) available. See DOI: 10.1039/d1ra00057h

‡ These authors equally contributed to the work.

solvent, the cocrystal may show inconsistent dissolution behavior, resulting in an asymmetric ternary phase diagram. Under the guidance of the asymmetric ternary phase diagram, the starting solution composition in the cocrystal region should be adjusted to prepare the cocrystal, which undoubtedly makes the cocrystal production difficult. If the two pure components have a similar solubility in the selected solvent, the cocrystal may show congruent dissolution behavior, resulting in a symmetric ternary phase diagram. Under the guidance of the symmetrical ternary phase diagram, the cocrystal can be prepared by simple cooling crystallization. Therefore, to develop industrial-scale preparation cocrystal, studying the symmetry of ternary phase diagram is a simple and reliable method. In addition, the temperature will directly affect the solubility of the two pure components in the solvent, which will undoubtedly have a certain impact on the thermodynamically stable region of the cocrystal in the ternary phase diagram.[37]

In this work, the dissolution behavior of the 2HNIW·HMX cocrystal in different solvents was studied. The solid–liquid ternary phase diagrams of the cocrystal in acetonitrile and ethyl acetate were established at 15 °C and 25 °C. This work aims to study the influence of temperature and solvent on the dissolution behavior of the cocrystal and the appearance of the ternary phase diagrams. Under the guidance of the obtained ternary phase diagram, the appropriate points were selected from the thermodynamically stable cocrystal region, and the 2HNIW·HMX cocrystal was prepared and characterized.

Experimental section

Materials

Raw HNIW and HMX were purified by recrystallization using a solvent/non-solvent method. 2HNIW·HMX cocrystal was also prepared by the solvent/non-solvent (acetonitrile/distilled water) method. All solvents for the experiment were obtained from commercial in analytical grade and without further purifications, and the detailed information is listed in Table 1.

Equipment

Powder X-ray diffraction (PXRD) patterns were carried out on a MiniFlex 300/600 X-ray diffractometer (D2 Phaser, Bruker AXS Gmbh, Germany) in the reflection mode with Cu-Kα radiation (40 kV, 15 mA). Data were collected from $2\theta = 5°$ to 50° at a step size of 0.02°. Fourier Transform Infrared (FTIR) spectrometer was performed on a BRUKER TENSOR27 (BRUKER, Germany) with KBr pellets in the range of 4000–400 cm^{-1}. Scanning Electron Microscopy (SEM) analysis was examined by a VEGA3 LMH instrument. The samples were coated with a thin layer of gold before observation.

The solubilities of HNIW and HMX were investigated by high-performance liquid chromatography (HPLC) (LC-20AD, Shimadzu Corporation, Japan). A Welchrom HPLC column (5.0 μm, 150 mm × 4.6 mm ID) was used with methanol/water (70/30, v/v) as the mobile phase. The wavelength of ultraviolet light was set at 254 nm. The flow rate was 1.0 mL min^{-1}, and the injection volume for each sample was 10 μL per sample. Each experiment was repeated six times.

Construction of the ternary phase diagrams

Slurries of different compositions of HNIW and HMX were produced in 5 mL syringes, and agitated for 72 h in a water bath at the specified temperature (25 and 35 °C), during which each syringe should contain an appropriate amount of solid. Subsequently, the saturated solutions were separated through 0.22 μm PTFE filters. Aliquots of solutions were analyzed by HPLC, and the concentrations of HNIW and HMX were determined by the calibration curves. The solid phases were collected and characterized by PXRD and FTIR.

Invariant points are fixed solution concentrations at which two solid phases can exist together in equilibrium. The invariant points (C_1 or C_2) were determined at (HNIW + cocrystal) region or (HMX + cocrystal) region. These points were determined by equilibrating a slurry of the two mentioned solid forms, using the method described by Rodriguez-Hornedo *et al.*[38] The slurries were equilibrated for 72 h, after which the concentrations of HNIW and HMX were measured by HPLC.

Isothermal slurry crystallization

Based on the ternary phase diagrams, isothermal slurry conversion experiments were carried out for investigation of the preparation of 2HNIW·HMX cocrystal. The two points were selected inside the thermodynamic stability region of cocrystal

Table 1 Source and mass fraction purity of the materials used in this work

Materials	Source of supply	CAS number	Mass fraction purity	Analysis method
HNIW	Liaoning Qingyang Special Chemical Co., Ltd., China	135285-90-4	0.993	HPLC[a]
HMX	Liaoning Qingyang Special Chemical Co., Ltd., China	2691-41-0	0.992	HPLC[a]
Acetonitrile	Alfa Aesar, China	75-05-8	≥0.998	GC[b]
Ethyl acetate	Alfa Aesar, China	141-78-6	≥0.997	GC[b]
Butanone	Guangdong Guanghua Sci-Tech Co., Ltd., China	78-93-3	≥0.998	GC[b]
N,*N*-Dimethylformamide	Alfa Aesar, China	68-12-2	≥0.995	GC[b]
Dimethylacetamide	Alfa Aesar, China	127-19-5	≥0.995	GC[b]
Distilled water	A.S. Watson Group (Hong Kong) Ltd., China	7732-18-5	—	—

[a] HPLC is the high-performance liquid chromatography and the purities determined through HPLC in this work. [b] GC is the gas chromatography and the purities determined by the supplier.

Table 2 Measured solubility values of HMX and HNIW in acetonitrile and ethyl acetate

Solvent	T (°C)	Solubility (mol solute/solvent)		Solubility (mol L^{-1})		Standard deviation (mol L^{-1}) ($n = 4$)		Solubility ratio (HNIW/HMX)
		HMX	HNIW	HMX	HNIW	HMX	HNIW	
Acetonitrile	15	0.0025	0.0519	0.0630	0.8816	0.0013	0.0009	20.76
	25	0.0030	0.0598	0.0739	1.0152	0.0015	0.0015	19.93
Ethyl acetate	15	0.0072	0.1143	0.4248	1.2660	0.0022	0.0011	15.87
	25	0.0101	0.1080	0.7163	1.1720	0.0031	0.0016	10.69

in each phase diagram to establish the conditions for cocrystal formation by slurry conversion. Pure solid components and the solvent were mixed in proportions corresponding to the selected point and agitated for 72 h to establish the solid–liquid equilibrium. Then, the solid phases were separated from the solution, allowed to dry and characterized.

Results and discussion

Solubility measurements

The measured solubility values of HMX and HNIW in acetonitrile and ethyl acetate at 15 °C and 25 °C are given in Table 2, as averages of $n = 4$ experiments, together with standard deviations. As shown in Table 2, the solubility of HMX in the selected solvents and HNIW in acetonitrile showed an increasing trend with the increase of temperature. However, the solubility of HNIW in ethyl acetate showed the opposite phenomenon, that is, it decreased with increasing temperature, which is consistent with the experimental results in the literature.[39]

It is worth noting that at 25 °C, the solubility values of HNIW in ethyl acetate and acetonitrile are about 10 times and 20 times that of HMX, respectively. Obviously, the solubility ratio values of HNIW and HMX in these two solvents showed a significant difference, but the differences of solubility of HNIW and HMX are both an order of magnitude. Therefore, it is desirable to obtain an asymmetric phase diagram in acetonitrile with a larger solubility ratio and an asymmetric phase diagram in ethyl acetate with a smaller solubility ratio.

Construction of the ternary phase diagrams

In order to gain some insights into the thermodynamics and phase behavior of the 2HNIW·HMX cocrystal in different solvents, the ternary phase diagrams of the cocrystal in acetonitrile and ethyl acetate were established at 15 and 25 °C. For clarity, the solubility of the two pure components and the invariant points in different solutions were converted to mass fraction and plotted on ternary axis diagrams to generate the appropriate ternary phase diagrams.

Ternary phase diagram for HMX–HNIW–acetonitrile system at 15 °C and 25 °C were constructed, respectively (Fig. 1 and 2). As expected, HMX and HNIW showed inconsistent dissolution behavior in acetonitrile, a trend that is common when there is a wide difference between the two pure components.

The phase diagram at 15 °C (Fig. 1) is divided into six regions. Region 1 represents an undersaturated solution phase, and all other regions have consisted of saturated solutions in contact with it. Region 2, 4, and 6 signify a solution in equilibrium with solid phases of HMX (blue filled), 2HNIW·HMX cocrystal (orange filled), and HNIW (yellow filled), respectively. As for regions 3 and 5, they signify the co-existence of cocrystal with HMX and HNIW, respectively. The blue dotted line is the 2 : 1 (HNIW : HMX) stoichiometric line. The invariant points

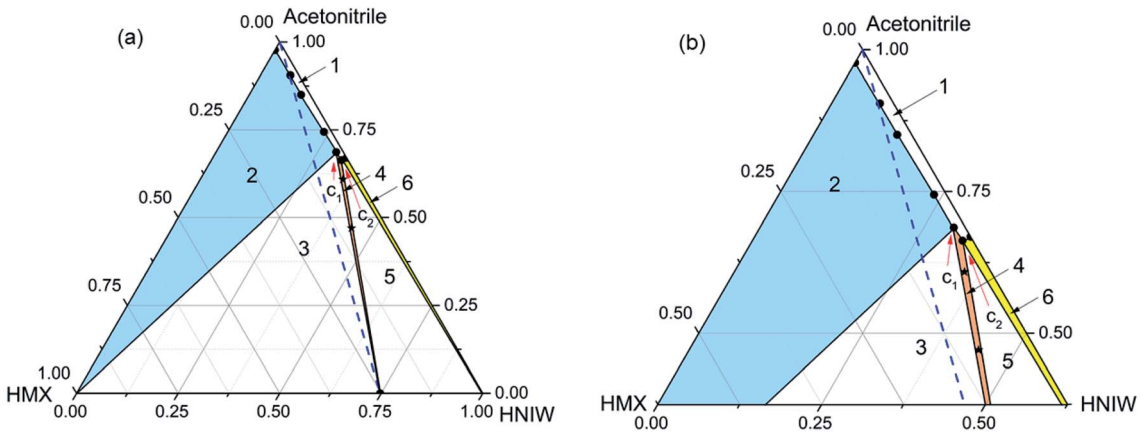

Fig. 1 Ternary phase diagram (a) and the expansion of the diagram (b) for HMX–HNIW–acetonitrile system at 15 °C. The points (black stars) represent starting compositions for cocrystal.

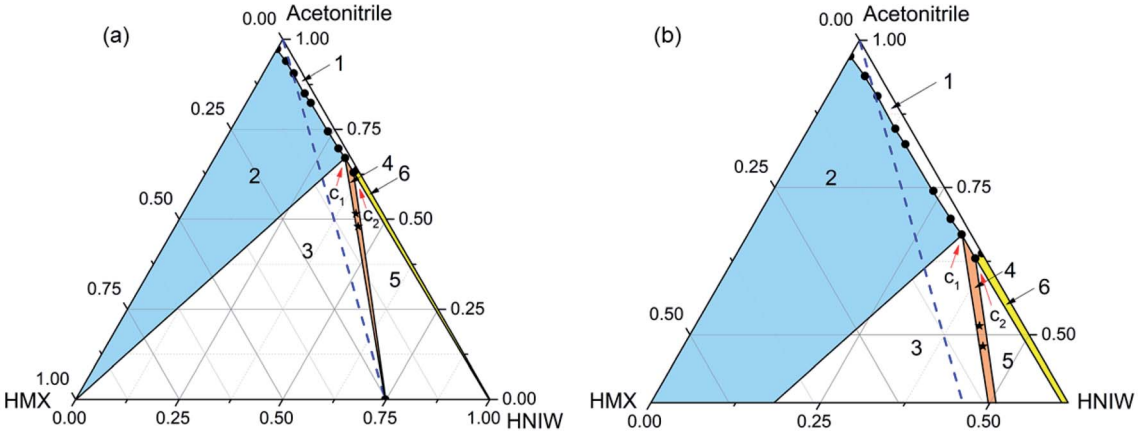

Fig. 2 Ternary phase diagram (a) and the expansion of the diagram (b) for HMX–HNIW–acetonitrile system at 25 °C. The points (black stars) represent starting compositions for cocrystal.

(C_1 and C_2) in the phase diagram were determined experimentally and expressed by a mass fraction, as shown in Table 3.

As shown in Fig. 1, the cocrystal stable region (region 4) inclines obviously to the HNIW axis as the solubility of HNIW is much higher than that of HMX (Table 2). The 2 : 1 (HNIW : HMX) component stoichiometric line does not intersect with the 2HNIW·HMX cocrystal solubility curve, resulting in an asymmetric phase diagram. This means that no matter how much acetonitrile is used, for a mixture with a 2 : 1 molar ratio of HNIW and HMX, a suspension of pure 2HNIW·HMX cocrystals cannot be obtained. This is because depending on the amount of solvent used, the cocrystal would eventually transform to the stable solid phase, *i.e.*, a mixture of cocrystal + HMX (region 3) or cocrystal + HNIW (region 5). That is, it is impossible to establish the solid–liquid equilibrium between the cocrystal solid phase and the stoichiometric solution. As a result, the solubility of the cocrystal cannot be readily determined as it transforms into the stable solid phase.[40,41]

The phase diagram (Fig. 2) has the same area at 25 °C. Compared with Fig. 1, the cocrystal solid-state phase region (region 4) in Fig. 2 has become larger. This is because the solubility of HMX and HNIW increased with the increasing temperature. As shown in Table 2, although the increasing temperature has increased the solubilities of the two pure components by different amounts, the effect of temperature increase on the solubility of HMX and HNIW is less obvious. This is why the size and position of other solid-state phase regions did not change significantly as the temperature increased. Therefore, Fig. 2 showed the same asymmetry as Fig. 1. Although the cocrystal still dissolved incongruently, the 2HNIW·HMX cocrystal can be prepared by selecting an appropriate point from the diagram.

For the HMX–HNIW–acetonitrile system, the change of temperature has a certain effect on the size and position of the thermodynamically stable cocrystal region, but it will not have any significant effect on the overall appearance of the phase diagram.

Ternary phase diagrams for HMX–HNIW–ethyl acetate system at 15 °C and 25 °C were constructed, respectively (Fig. 3 and 4). Regions in the diagram are as same as marked in Fig. 1. The blue dotted line is the 2 : 1 (HNIW : HMX) stoichiometric line. The invariant points (C_1 and C_2) in the phase diagram were determined experimentally and expressed by a mass fraction, as shown in Table 4.

Unlike the acetonitrile system, HMX and HNIW showed consistent dissolution behavior in ethyl acetate. It can be seen

Table 3 Invariant points of HMX and HNIW in acetonitrile

			Invariant point (mass fraction)	
Solvent	T (°C)	Solid phase in equilibrium	HMX	HNIW
Acetonitrile	15	HMX + cocrystal	0.0175	0.2958
		HNIW + cocrystal	0.0157	0.3209
	25	HMX + cocrystal	0.0141	0.3152
		HNIW + cocrystal	0.0141	0.3558

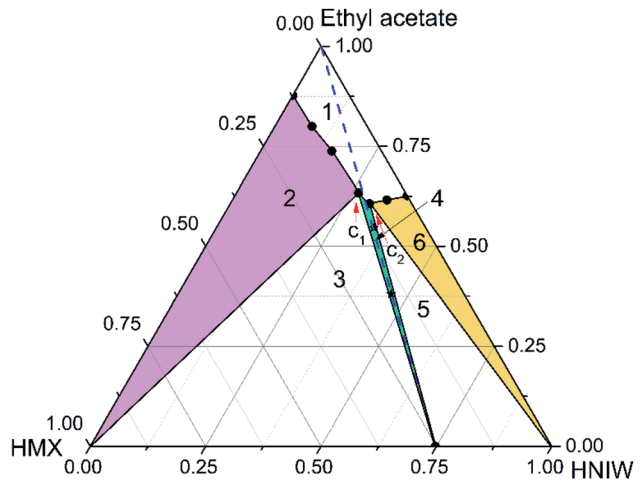

Fig. 3 Ternary phase diagram for HMX–HNIW–ethyl acetate system at 15 °C. The points (black stars) represent starting compositions for cocrystal.

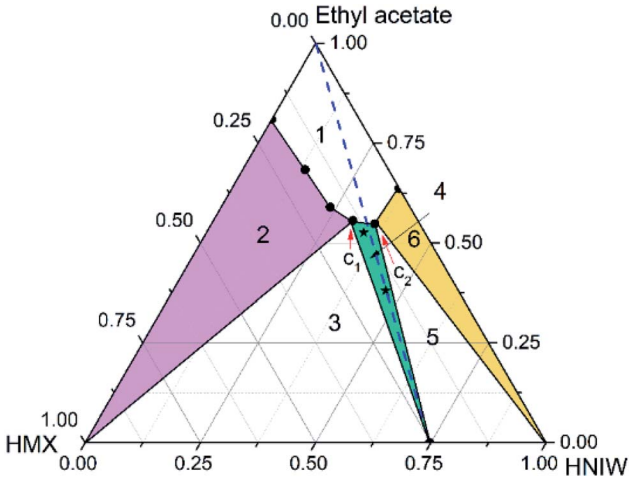

Fig. 4 Ternary phase diagram for HMX–HNIW–ethyl acetate system at 25 °C. The points (black stars) represent starting compositions for cocrystal.

from Table 2 that the solubility of HNIW is about 10 times that of HMX, which means that there is a significant difference between the two pure components. Generally, when there is a significant difference between the two components, it is easier to exhibit inconsistent dissolution behavior in the solvent. However, in this work, HNIW and HMX showed consistent dissolution behavior, despite their large solubility differences.

Compared with the acetonitrile system, the appearance of the phase diagram changed considerably. For instance, the undersaturated solution region (region 1) is larger than in acetonitrile, the solid-state region of cocrystal (region 4, green filled) and HNIW (region 6, yellow filled) get larger, the solid-state region of HMX (region 1, purple filled) get smaller, the distance between the solvent peak and the cocrystal solubility curve becomes longer, the 2 : 1 (HNIW : HMX) component stoichiometric line intersected with the 2HNIW·HMX cocrystal solubility curve, and the phase diagram showed the congruent dissolution behavior. These changes are due to the solubility difference between HNIW and HMX in ethyl acetate has been reduced. Simultaneously, since this difference still has an order of magnitude, the cocrystal stable region (region 4) is tilted to the HNIW axis.

Compared with the phase diagram at 15 °C, the various solid regions in the ternary phase diagram moved downward, and the undersaturated solution phase (region 1) and cocrystal solid phase (region 4) occupied broader regions. It can be seen from Table 2, as the temperature increased, the solubility of HMX increased, while the solubility of HNIW decreased. The increasing temperature has a more noticeable effect on the solubility of HMX, resulting in a larger cocrystal stable region near the HMX side. Since the cocrystal dissolved congruently, the solubility of 2HNIW·HMX cocrystal can be determined gravimetrically. Based on eqn (1) (ESI†) the measured solubility values of the cocrystal in ethyl acetate at 15 °C and 25 °C were 0.0862 and 0.0884, respectively. The results show that the choice of solvent has a crucial influence on the dissolution behavior of the cocrystal and the size and position of each region in the phase diagram. Although the temperature has no apparent effect on the overall appearance of the phase diagram, it could affect the size of the thermodynamically stable region of the cocrystal.

The experimental results show that the dissolution behavior of the cocrystal cannot be predicted only by the solubility of the two pure components of the cocrystal in the solvent. In other words, the solubility of the two pure components of the cocrystal in the solvent cannot be used to reliably predict whether the dissolution behavior of the cocrystal is consistent or inconsistent. Compared with the temperature, the solvent plays a vital role in affecting the dissolution behavior of the cocrystal system. In addition, the experimental results of the 2HNIW·HMX cocrystal ternary phase diagram have special guiding significance for the development of industrial-scale cocrystal manufacturing. Based on the consistent dissolution behavior of the cocrystal in ethyl acetate, the cocrystal could be prepared by simple cooling crystallization, which significantly simplifies the cocrystal preparation process in industrial production.

Table 4 Invariant points of HMX and HNIW in ethyl acetate

Solvent	T (°C)	Solid phase in equilibrium	Invariant point (mass fraction) HMX	HNIW
Ethyl acetate	15	HMX + cocrystal	0.1016	0.2649
		HNIW + cocrystal	0.0919	0.3015
	25	HMX + cocrystal	0.1413	0.3024
		HNIW + cocrystal	0.0978	0.3543

Isothermal slurry co-crystallization

In order to prove the reliability of ternary phase diagrams, the most effective method is to select the combination points from the thermodynamically stable region of the cocrystal to prepare

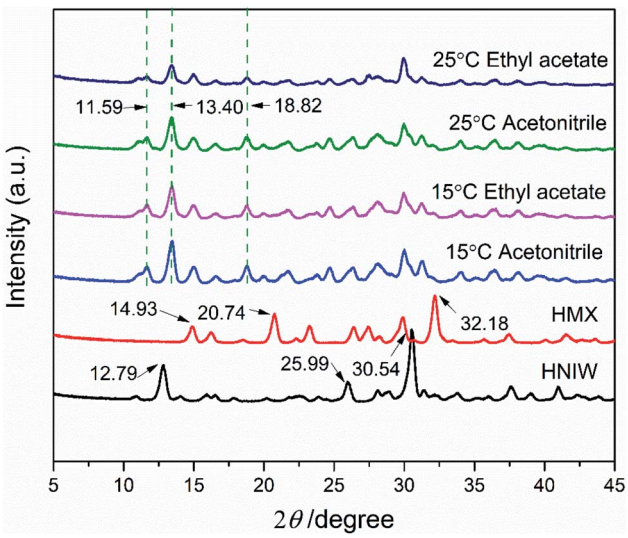

Fig. 5 PXRD patterns of 2HNIW·HMX cocrystal prepared by isothermal slurry co-crystallization method.

the cocrystal. In region 4 of each ternary phase diagram, the points represented by the star symbol were selected to prepare the 2HNIW·HMX cocrystal by the isothermal slurry conversion crystallization method in acetonitrile and ethyl acetate. Powder X-ray diffraction (PXRD) patterns of cocrystals obtained by this method from the different experimental conditions at equilibrium are shown in Fig. 5. It can be seen from the figure that the PXRD curves of the cocrystal overlap to a large extent with the curves of the two pure components, but at the same time, they also show some differences. For example, the diffraction peaks at 2θ of 12.8°, 26.0°, 30.7° of pure HNIW and those at 2θ of 14.7°, 20.4°, 31.9° of pure HMX disappeared in the cocrystal curve, and the new sharp diffraction peaks at 2θ of 11.65°, 13.40°, 18.76° emerged in the cocrystal curve. Such differences can be attributed to the formation of cocrystals. The results of the FTIR spectrum of 2HNIW·HMX cocrystal are shown in Fig. 6. To a large extent, they are the superposition of the HMX and HNIW spectra, while some differences exist. The C–H stretching bands of HNIW appear at 3040 and 3016 cm^{-1}, and that of HMX are at 3030 and 2985 cm^{-1}. However, the C–H stretching vibration of cocrystal has a certain degree of displacement. FTIR spectra of cocrystal have significant differences in the range of 1435–1410 cm^{-1} compared to the HNIW and HMX. The major difference is that the cocrystal exhibits low-intensity peaks, which may be caused by the formation of the hydrogen bonds.[42,43] The results of FTIR spectra confirm the formation of 2HNIW·HMX cocrystal as the supplement of PXRD. SEM analysis was carried out to compare the external appearance of HMX, HNIW, and cocrystal (Fig. S3†). The results show that HMX and HNIW exhibit polyhedral prismatic shape and irregular spindle shape, respectively. However, the obtained 2HNIW·HMX cocrystal could be differentiated by its prismatic crystal shape. Therefore, the difference in external appearance between the cocrystal and the two pure components indicates that the cocrystal has a new microstructure. Compared with the ref. 44, the characterization results (SEM and PXRD) of the 2HNIW·HMX cocrystal are consistent with the results in the reference, which further approved the successful preparation of 2HNIW·HMX cocrystal instead of its mixture.

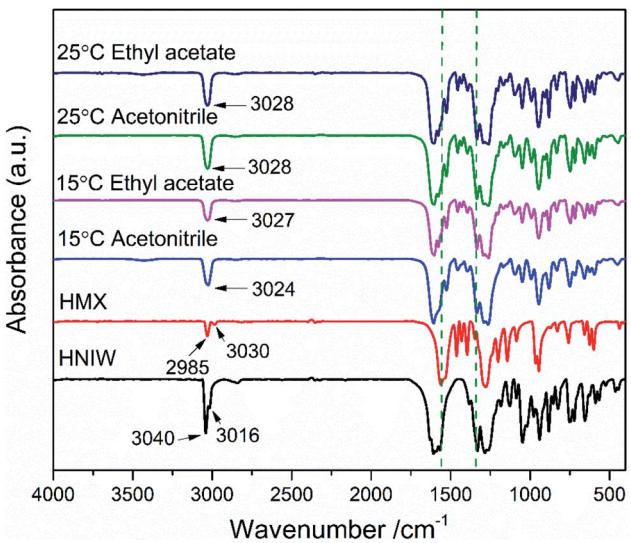

Fig. 6 FTIR spectra of 2HNIW·HMX cocrystal prepared by isothermal slurry co-crystallization method.

Conclusions

Ternary phase diagrams of the 2HNIW·HMX cocrystal in acetonitrile and ethyl acetate were established at 15 °C and 25 °C. HMX and HNIW exhibited inconsistent dissolution behavior and congruent dissolution behavior in acetonitrile and ethyl acetate, respectively. The solvent has a crucial influence on the cocrystal dissolution behavior and can significantly affect the width of the cocrystal stable region. The 2HNIW·HMX cocrystal has a narrow thermodynamically stable region in acetonitrile and a wider thermodynamically stable region in ethyl acetate. The results showed that the appearance of the phase diagram depends strongly on the choice of solvent, and the temperature has a weak effect on the phase diagram. Under the guidance of the phase diagram, the 2HNIW·HMX cocrystal has been prepared by isothermal slurry conversion crystallization method and characterized.

Conflicts of interest

There are no conflicts to declare.

Acknowledgements

We gratefully acknowledge the financial support from the National Natural Science Foundation of China (grant numbers 21673182 and 21703168) and the Fund of China Ordnance Industry Group Fourth Institute (Contract Record Number: 2020HX0882, Contract No. 204-J-2020-1265-1/6).

References

1 G. Y. Huang, W. L. Yu, T. Wang, J. T. Wang and L. Zhen, Theoretical insights into effects of molar ratios on stabilities, mechanical properties and detonation performance of CL-20/RDX cocrystal explosives by molecular dynamics simulation, *J. Mol. Struct.*, 2017, **1141**, 577–583.

2 Q. Jia, J. Q. Zhang, K. C. Kou, S. J. Zhang and Y. L. Xu, Preparation, characterization and the thermodynamic properties of HNIW·TNT cocrystal, *Propellants, Explos., Pyrotech.*, 2019, **44**, 588–596.

3 P. Y. Chen, L. Zhang, S. G. Zhu, G. B. Cheng and N. R. Li, Investigation of TNB/NNAP cocrystal synthesis, molecular interaction and formation process, *J. Mol. Struct.*, 2017, **1128**, 629–635.

4 A. McBain, V. Vuppuluri, I. E. Gunduz, L. J. Groven and S. F. Son, Laser ignition of CL-20 (hexanitrohexaazaisowurtzitane) cocrystals, *Combust. Flame*, 2018, **188**, 104–115.

5 O. Bolton and A. J. Matzger, Improved Stability and Smart-Material Functionality Realized in an Energetic Cocrystal, *Angew. Chem., Int. Ed.*, 2011, **50**, 8960–8963.
6 H. F. Gao, S. H. Zhang, F. D. Ren, F. Liu, R. J. Gou and X. Ding, Theoretical insight into the co-crystal explosive of 2,4,6,8,10,12-hexanitrohexaazaisowurtzitane (CL-20)/1,1-diamino-2,2-dinitroethylene (FOX-7), *Comput. Mater. Sci.*, 2015, **107**, 33–41.
7 H. W. Qiu, R. B. Patel, R. S. Damavarapu and V. Stepanov, Nanoscale 2CL-20·HMX high explosive cocrystal synthesized by bead milling, *CrystEngComm*, 2015, **17**, 4080–4083.
8 H. Qiu, V. Stepanov, A. R. Di Stasio, T. Chou and W. Y. Lee, RDX-based nanocomposite microparticles for significantly reduced shock sensitivity, *J. Hazard. Mater.*, 2011, **185**, 489–493.
9 T. Chen, W. Jiang, P. Du, J. Liu, G. Hao, H. Gao, L. Xiao and X. Ke, Facile preparation of 1,3,5,7-tetranitro-1,3,5,7-tetrazocane/glycidylazide polymer energetic nanocomposites with enhanced thermolysis activity and low impact sensitivity, *RSC Adv.*, 2017, **7**, 5957–5965.
10 G. He, Z. Yang, X. Zhou, J. Zhang, L. Pan and S. Liu, Polymer bonded explosives (PBXs) with reduced thermal stress and sensitivity by thermal conductivity enhancement with graphene nanoplatelets, *Compos. Sci. Technol.*, 2016, **131**, 22–31.
11 S. J. Zhang, Z. G. Gao, Q. Jia, N. Liu, J. Q. Zhang and K. C. Kou, Fabrication and characterization of surface modified HMX@PANI core–shell composites with enhanced thermal properties and desensitization *via in situ* polymerization, *Appl. Surf. Sci.*, 2020, **515**, 146042.
12 T. M. Klapötke, F. A. Martin and J. Stierstorfer, C_2N_{14}: an energetic and highly sensitive binary azidotetrazole, *Angew. Chem., Int. Ed.*, 2011, **50**, 4227–4229.
13 D. J. Good and N. Rodríguezhornedo, Solubility advantage of pharmaceutical cocrystals, *Cryst. Growth Des.*, 2009, **9**, 2252–2264.
14 D. Hasa, R. G. Schneider, D. Voinovich and W. Jones, Cocrystal formation through mechanochemistry: from neat and liquid-assisted grinding to polymer-assisted grinding, *Angew. Chem., Int. Ed.*, 2015, **54**, 7371–7375.
15 N. K. Duggirala, M. L. Perry, Ö. Almarsson and M. J. Zaworotko, Pharmaceutical cocrystals: along the path to improved medicines, *Chem. Commun.*, 2016, **52**, 640–655.
16 K. Liu, G. Zhang, J. Luan, Z. Chen, P. Su and Y. Shu, Crystal structure, spectrum character and explosive property of a new cocrystal CL-20/DNT, *J. Mol. Struct.*, 2016, **1110**, 91–96.
17 G. Hang, W. Yu, T. Wang, J. Wang and Z. Li, Comparative studies on structures, mechanical properties, sensitivity, stabilities and detonation performance of CL-20/TNT cocrystal and composite explosives by molecular dynamics simulation, *J. Mol. Model.*, 2017, **23**, 281.
18 D. Guo, Q. An, S. V. Zybin, W. A. Goddard III, F. Huang and B. Tang, The co-crystal of TNT/CL-20 leads to decreased sensitivity toward thermal decomposition from first principles based reactive molecular dynamics, *J. Mater. Chem. A*, 2015, **3**, 5409–5419.
19 S. J. Zhang, Z. G. Gao, D. Lan, Q. Jia, N. Liu, J. Q. Zhang and K. C. Kou, Recent advances in synthesis and properties of nitrated-pyrazoles based energetic compounds, *Molecules*, 2020, **25**, 3475.
20 Q. Jia, D. Lei, S. J. Zhang, J. Q. Zhang, N. Liu and K. C. Kou, Solubility measurement and correlation for HNIW·TNT co-crystal in nine pure solvents from $T = (283.15$ to $318.15)$ K, *J. Mol. Liq.*, 2020, 114592.
21 P. H. Lv, H. Y. Wang, L. P. Dang, C. H. Sun and S. P. Pang, Measurement and correlation of solubility of ε-CL-20 in solvent mixtures of (chloroform + ethyl acetate) and (*m*-xylene + ethyl acetate) at temperatures from 278.15 K to 313.15 K, *J. Mol. Liq.*, 2017, **231**, 192–201.
22 Q. Jia, J. Q. Zhang, S. J. Zhang, Q. Shi, D. Lei, Y. L. Xu and K. C. Kou, Low-temperature heat capacities, standard molar enthalpies of formation and detonation performance of two CL-20 co-crystal energetic materials, *Fluid Phase Equilib.*, 2020, **518**, 112638.
23 Z. J. Yang, L. Ding, P. Wu, Y. G. Liu, F. D. Nie and F. L. Huang, Fabrication of RDX, HMX and CL-20 based microcapsules *via in situ* polymerization of melamine–formaldehyde resins with reduced sensitivity, *Chem. Eng. J.*, 2015, **268**, 60–66.
24 Y. F. Zhu, Y. W. Lu, B. Gao, D. J. Wang, G. C. Yang and C. P. Guo, Ultrasonic-assisted emulsion synthesis of well-distributed spherical composite CL-20@PNA with enhanced high sensitivity, *Mater. Lett.*, 2017, **205**, 94–97.
25 S. J. Zhang, Z. G. Gao, Q. Jia, N. Liu, J. Y. Yao, J. Q. Zhang and K. C. Kou, Bioinspired strategy for HMX@hBNNS dual shell energetic composites with enhanced desensitization and improved thermal property, *Adv. Mater. Interfaces*, 2020, **7**, 2001054.
26 O. Bolton, L. R. Simke, P. F. Pagoria and A. J. Matzger, High power explosive with good sensitivity: A 2 : 1 cocrystal of CL-20 : HMX, *Cryst. Growth Des.*, 2012, **12**, 4311–4314.
27 M. Eraković, V. Nemec, T. Lež, I. Porupski, V. Stilinović and D. Cinčić, Halogen Bonding of *N*-Bromophthalimide by Grinding and Solution Crystallization, *Cryst. Growth Des.*, 2018, **18**, 1182–1190.
28 S. P. Patil, S. R. Modi and A. K. Bansal, Generation of 1 : 1 Carbamazepine : Nicotinamide cocrystals by spray drying, *Eur. J. Pharm. Sci.*, 2014, **62**, 251–257.
29 A. Mukherjee, R. D. Rogers and A. S. Myerson, Cocrystal formation by ionic liquid-assisted grinding: case study with cocrystals of caffeine, *CrystEngComm*, 2018, **20**, 3817–3821.
30 D. Hasa, R. G. Schneider, D. Voinovich and W. Jones, Cocrystal Formation through Mechanochemistry: from Neat and Liquid-Assisted Grinding to Polymer-Assisted Grinding, *Angew. Chem., Int. Ed.*, 2015, **54**, 7371–7375.
31 C. Hong, Y. Xie, Y. S. Yao, G. W. Li, X. R. Yuan and H. Y. Shen, A novel strategy for pharmaceutical cocrystal generation without knowledge of stoichiometric ratio: myricetin cocrystals and a ternary phase diagram, *Pharm. Res.*, 2015, **32**, 47–60.
32 M. D. Croker, E. M. Foreman, N. B. Hogan, M. N. Maguire, J. C. Elcoate, K. B. Hodnett, R. A. Maguire, C. Å. Rasmuson

and E. S. Lawrence, Understanding the *p*-toluenesulfonamide/triphenylphosphine oxide crystal chemistry: A new 1 : 1 cocrystal and ternary phase diagram, *Cryst. Growth Des.*, 2012, **12**, 869–875.

33 H. Veith, M. Schleinitz, C. Schauerte and G. Sadowski, Thermodynamic approach for co-crystal screening, *Cryst. Growth Des.*, 2019, **19**, 3253–3264.

34 C. Loschen and A. Klamt, Cocrystal ternary phase diagrams from density functional theory, *Cryst. Growth Des.*, 2018, **18**, 5600–5608.

35 S. Darwish, J. Zeglinski, G. R. Krishna, R. Shaikh, M. Khraisheh, G. M. Walker and D. M. Croker, A New 1 : 1 Drug–Drug Cocrystal of Theophylline and Aspirin: Discovery, Characterization, and Construction of Ternary Phase Diagrams, *Cryst. Growth Des.*, 2018, **18**, 7526–7532.

36 Q. Jia, J. Q. Zhang, S. J. Zhang, D. Lei, Y. L. Xu and K. C. Kou, Investigation of the phase behavior of a HNIW·TNT cocrystal system and construction of ternary phase diagrams, *Cryst. Growth Des.*, 2019, **19**, 6370–6376.

37 D. Ahuja, M. Svärd and Å. C. Rasmuson, Investigation of solid–liquid phase diagrams of the sulfamethazine–salicylic acid co-crystal, *CrystEngComm*, 2019, **21**, 2863–2874.

38 D. J. Good and R. H. Naír, Solubility Advantage of Pharmaceutical Cocrystals, *Cryst. Growth Des.*, 2009, **9**, 2252–2264.

39 P. Lv, H. Wang, Y. Tong, L. Dang, C. Sun and S. Pang, Measurement and Correlation of the Solubility of ε-CL-20 in 12 Organic Solvents at Temperatures Ranging from 278.15 to 318.15 K, *J. Chem. Eng. Data*, 2017, **62**, 961–966.

40 S. Zhang, H. Chen and Å. C. Rasmuson, Thermodynamics and crystallization of a theophylline–salicylic acid cocrystal, *CrystEngComm*, 2015, **17**, 4125–4135.

41 M. M. Bishop, N. Velisavljevic, R. Chellappa and Y. K. Vohra, High Pressure–Temperature Phase Diagram of 1,1-Diamino-2,2-dinitroethylene (FOX-7), *J. Phys. Chem. A*, 2015, **119**, 9739–9747.

42 P. Sharma, M. M. Sundaram, D. Singh and R. Ahuja, Highly Energetic and Stable Gadolinium/Bismuth Molybdate with a Fast Reactive Species, Redox Mechanism of Aqueous Electrolyte, *ACS Appl. Energy Mater.*, 2020, **3**, 12385–12399.

43 M. M. Sundaram and D. Appadoo, Traditional salt-in-water electrolyte *vs.* water-in-salt electrolyte with binary metal oxide for symmetric supercapacitors: capacitive *vs.* faradaic, *Dalton Trans.*, 2020, **49**, 11743–11755.

44 W. Pang, K. Wang, W. Zhang, L. T. Luca, X. Fan and J. Li, CL-20-Based Cocrystal Energetic Materials Simulation, Preparation and Performance, *Molecules*, 2020, **25**, 4311.